photonics

MDPI

Communication

Research on A High-Sensitivity Temperature Sensor with Multi-Indicator Based on Nano-Cylinder-Loaded Ring Resonator

Peng Zhou[1], Kun Liang [1], Yilin Wang [2], Qing'an Sun [1], Jiaqi Guo [3], Lei Jin [1] and Li Yu [1,*]

[1] Key Laboratory of Information Photonics and Optical Communications, School of Science, Beijing University of Posts and Telecommunications, Beijing 100876, China
[2] College of Mathematics and Physics, Beijing University of Chemical Technology, Beijing 100029, China
[3] School of Physics, PeKing University, Beijing 100871, China
* Correspondence: yuliyuli@bupt.edu.cn

Abstract: Increasing sensor sensitivity and maintaining a large FOM (figure of merit) are challenging to achieve at the same time. Adding grooves and asymmetrical structures to the annular cavity increases sensitivity; however, it usually makes the FOM of the structure decrease. Herein, we propose a MIM (metal-insulator-metal) sensor of a novel structure with nano-cylinders loaded in a ring resonator (NCRR), whose sensitivity can reach as high as 3636.4 nm/RIU (refractive index unit). The FOM is maintained around 2000 in the mid-infrared (MIR) region. We find that grating effects only occur in the ring cavity when the cylinder's distance is below three times its radius, and it can improve the sensitivity of the proposed structure up to 42.3% without decreasing its FOM. In addition, results suggest that our sensor has excellent resistance to eccentricity, which brings in manufacturing. Furthermore, we investigate the capability of the proposed device as a temperature sensor with ethanol, which exhibits a maximum temperature sensitivity of 1.48 nm/°C. We believe that our research has essential application prospects in miniature integrated sensors, optical switches, splitters, filters, and broadband passers.

Keywords: array of nano-dots; refractive index sensor; asymmetrical breakage; high resolution

Citation: Peng, Z.; Liang, K.; Wang, Y.; Sun, Q.; Guo, J.; Jin, L.; Yu, L. Research on A High-Sensitivity Temperature Sensor with Multi-Indicator Based on Nano-Cylinder-Loaded Ring Resonator. *Photonics* **2023**, *10*, 69. https://doi.org/10.3390/photonics10010069

Received: 30 November 2022
Revised: 26 December 2022
Accepted: 2 January 2023
Published: 8 January 2023

1. Introduction

Surface plasmon polaritons (SPPs) are transverse electromagnetic (TM) waves that propagate along the metal-dielectric interface and decay exponentially away from the metal-dielectric juncture. Since SPPs can place the local energy area beyond the diffraction limit in light-matter interactions, they have been considered a perfect potential information carrier to overcome the diffraction limit of light in future optical integrated circuits. Moreover, SPPs have a swift and sensitive response to changes in the ambient medium, which opens up new aspects in RI (refractive index) sensing applications. They can tune light-metal interactions and have a wide range of applications in filters [1–3], splitters [4], absorbers, sensors [5,6], switches [7], and other light-on-chip systems.

Optical signals have transmission flexibility, anti-interference abilities, high sensitivity, and relatively low costs. They are a better carrier to detect background changes in sensors than other targets [8]. Temperature sensors based on MIM structures stand out because SPPs can change the ambient temperature of the physical background signal into a noticeable change in the optic spectrum. Nevertheless, an SPP sensor is easy to combine with other light-on-a-chip systems, such as filters and switchers, and has high-resolution sensitivity. By exploring the relationship between the refractive index and the optical spectral lines, we can design an optical sensor device with high resolution that can detect ambient targets, such as temperature, pressure, and molecular concentration.

In this paper, we design a novel high-resolution temperature sensor based on the MIM structure [9–11]. It comprises a ring cavity studded with an array of silver nano-cylinders and a tiny cavity made by two silver walls in the propagating waveguide. We use the 2D finite element method (FEM) simulation (COMSOL 5.6) to optimize the parameters of the structure, and the silver cylinder grating structure can increase the sensitivity up to 42.3% without decreasing its FOM. Our structure can achieve a sensitivity **S** as high as 3636.4 nm/RIU in the mid-infrared region (MIR, at about 5 um), and its FOM is maintained at 2000 when the ring cavity is in fundamental mode. Compared to these proposed temperature sensors [12,13], stubs and grooves have been used to increase temperature sensitivity, while the FOM usually decreases to 100 or below. Our results have a significant advantage over other temperature sensors [14,15]. We believe that our research may bring inspiration to other broadband passers [16], switchers [17], and filters [13,18] that have a similar structural design.

2. Sensor Schematic and Theoretical Analysis

In FEM simulations, three-dimensional simulations are calculated according to the parameters of the structures, but their calculation time is very long, and additionally, the requirements for server configuration are also very high. Conversely, two-dimensional simulations treat the thickness of the structure as infinite, saving much computer memory by calculating the electromagnetic field's evolution in a two-dimensional plane. Some works have mentioned before that for a TM (transverse magnetic) mode in a MIM structure, 2D or 3D simulations make little difference during propagation. As the thickness **h** increases, the results of the 3D simulation and 2D simulation converge, and the results tend to remain stable with h greater than 100 nm [19]. Therefore, the final result of the 2D simulation can be trusted. In this paper, a plane wave at the input port excites the TM mode of the MIM waveguide. Thus, the transmittance of power is calculated as T = output power (Po)/input power (Pi).

The three-dimensional schematic of the proposed structure is illustrated in Figure 1a, where the grey and transparent zones represent silver and the material under sensing (MUS), respectively. The reason for choosing silver is that the loss of silver is relatively low. The structure consists of a waveguide coupled with a ring resonator. Two 5 nm thick silver blocks induce a broad continuum mode. The initial simulation parameters are tabulated in Table 1. Figure 1b illustrates the transmittance profile of the structure at a refractive index (n) of 1. We can observe several asymmetric Fano resonances named modes 2, 3, and 4 at the NIR and visible spectra. The name of the mode is derived from the different coherent orders in the resonant ring.

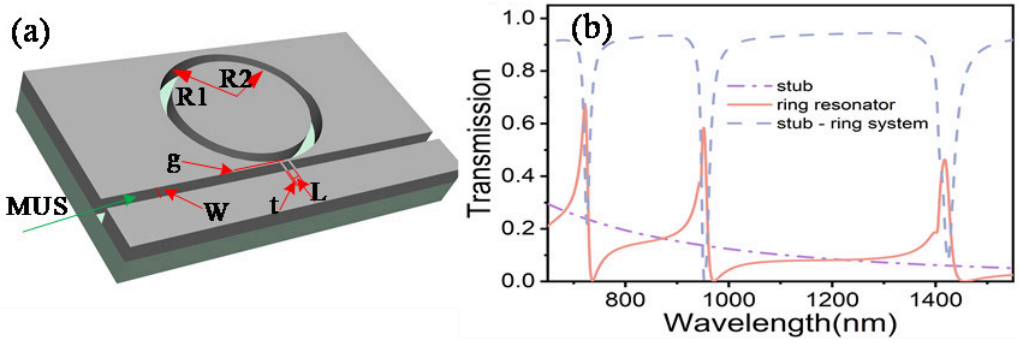

Figure 1. (**a**) 3D schematic of the proposed nanosensor. (**b**) Transmittance profile at n = 1. The purple dashed-dotted line, blue dashed line, and solid orange line represent the transmittance profile of the Fabry–Perot cavity, the ring resonator, and the system.

Table 1. Initial simulation parameters of the sensor.

Parameter	Symbol	Value
Waveguide width	w	50 nm
Inner radius	R1	300 nm
Outer radius	R2	350 nm
Radius of the nanorods	r	20 nm
Number of the nanorods	n	36
Waveguide gap width	g	10 nm
The thickness of the stub	t	5 nm
Distance between the stub	L	15 nm

At the NIR region, the complex permittivity of silver is wavelength dependent, which is characterized through the Drude model. The equation can be derived as $\mathrm{I}\varepsilon(\omega) = 1 - \frac{\omega_p^2}{\omega(\omega - i\Gamma_1)}$, where ω_p and Γ_1 are the plasma and resonant frequencies [9]. Table 2 presents the numerical values of these parameters.

Table 2. Drude parameter for silver.

Parameter	Value	Unit
Dielectric constant	3.7	1
Bulk plasma frequency	9.1	eV
Electron collision	0.018	eV
Incident frequency	1.24	eV

The corresponding t_i and k_i are transmission and coupling amplitudes of these two regions, where $t_i^2 + k_i^2 = 1$. The following equation can express the dispersion relation of SPPs in the MIM waveguide structure.

$$\varepsilon_d \sqrt{(\beta^2 - \varepsilon_m k_0^2)} + \varepsilon_m \sqrt{(\beta^2 - \varepsilon_d k_0^2)} \tanh\left(\omega \sqrt{(\beta^2 - \varepsilon_d k_0^2)})/2\right) = 0 \quad (1)$$

where ε_m is the complex dielectric constant of the background material, ε_d is the dielectric constant of the medium, $\beta = k_0 * n_{\mathrm{eff}}$ is the propagation constant of the SPPs, and $k_0 = 2\pi/\lambda$ is the wave vector of light in a vacuum.

In standing wave theory, the resonant wavelength is proportional to the effective refractive index and length (L) of the resonator, which can be defined as:

$$\lambda_{\mathrm{res}} = \frac{2\,\mathrm{Re}\left(n_{eff}\right)L}{M - \left(\frac{\varphi}{2\pi}\right)} M = 1, 2 \ldots \quad (2)$$

where M and ψ denote the mode integer and the phase shift due to reflection from the resonator, respectively. The sensing performance of the proposed nanosensor can be evaluated by the sensitivity value (S), which can be expressed as $\mathrm{S} = \frac{\Delta\lambda}{\Delta T}$, where $\triangle\lambda$ is the change in the resonance wavelength, and $\triangle T$ is the temperature change in the MUS. The figure of merit can be expressed as $\mathrm{FOM} = \frac{\Delta T}{\Delta n}$, where $\triangle T$ is the change in the transmission profile and $\triangle n$ is the refractive index change in the MUS.

3. Numerical Analysis and Optimization

3.1. Numerical Optimization

When the standard sensor is simulated in visible and near-infrared wavelength regions, three Fano resonances are obtained as shown in Figure 1b. Two thin silver walls excite a broad continuous spectrum in the waveguide, and ring-shaped resonators of different orders can produce a narrow linewidth dip in the transmission pattern. Both of these are coupled to form a Fano line pattern. Then, we explore the relationship be-

tween the coupling distance and the transmission pattern. The coupling strength can be tuned by adding the distance between the ring resonator and the waveguide, and λ_{res} remains stable. In Figure 2a, we can figure out that when the distance g is relatively small (5 nm), the coupling is strong to induce a dip in the transmission pattern and broaden the linewidth. When the coupling distance g becomes more significant, the linewidth becomes narrower, but the maximum transmission pattern decreases. This phenomenon is because the coupling between the two modes is weaker. To keep the Fano peak prominent in the transmission profile and linewidth narrower, we keep the coupling distance g = 10 nm. Since we keep the waveguide w = 50 nm in the whole structure, the outer radius of the ring resonator has no effect on sensitivity but only affects the transmittance peak wavelength, and we can adjust the resonator length to explore other ambient indicators.

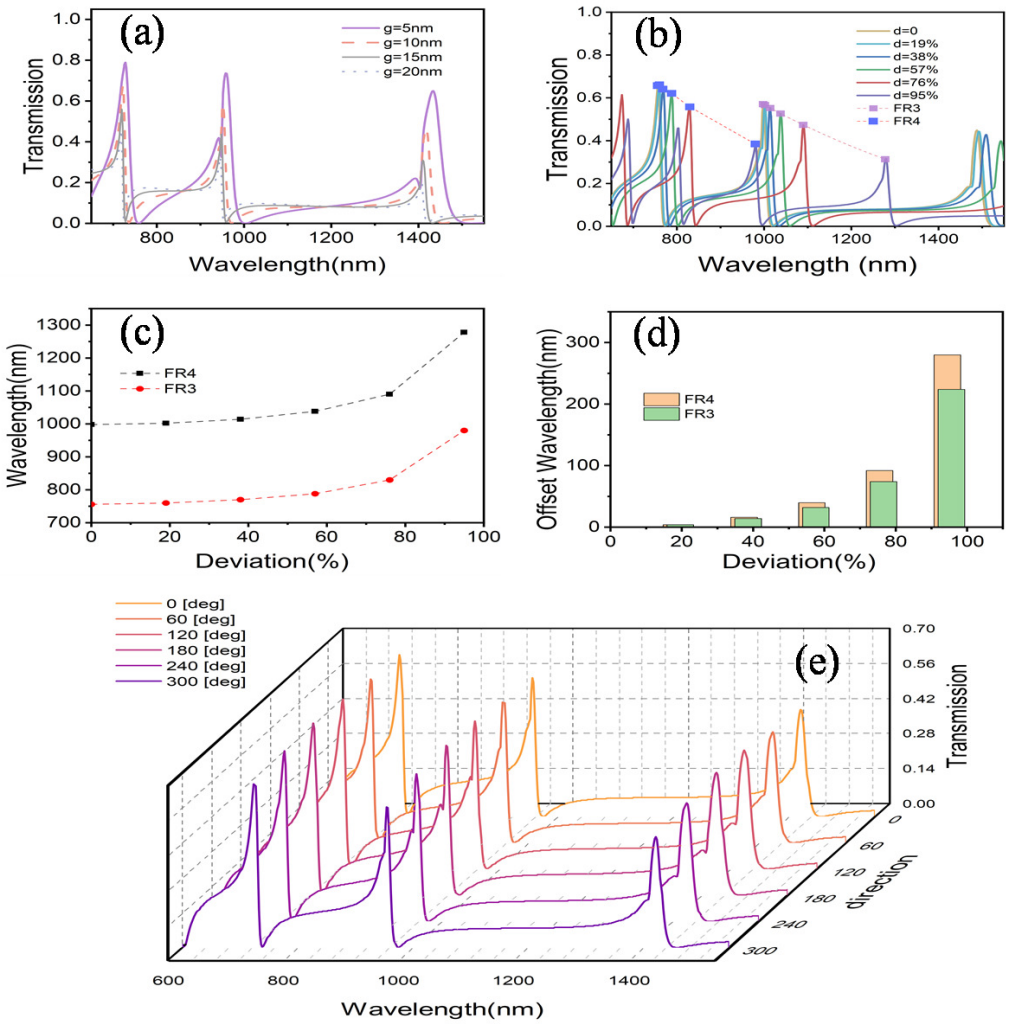

Figure 2. (**a**) Transmittance spectra for different coupling distances, g = 5 nm to g = 20 nm. (**b**) Transmittance spectra of the nanosensor with different eccentricity from 19–95%, where d = $\triangle r/w$. (**c**) The peak wavelength of FR3 and FR4 for different amplitude eccentric ring resonators in detail. (**d**) The offset in the peak wavelength of FR3 and FR4 in the annular cavity with different eccentricities. (**e**) Transmittance spectra of the nanosensor with different eccentric directions. When eccentricity amplitude is fixed, the direction does not change the transmission profile.

From a practical point of view, we also studied the effect of eccentricity due to processing on the transmission pattern. We defined the distance between the center of the inner circle and the outer circle as $\triangle r$; w is the waveguide width, and the eccentricity of the ring resonator d = $\triangle r/w$. We set the eccentricity d from 0 to 95% nm at 19% intervals, then

studied the effect of 6 different sets on the transmission pattern. By looking at the magnetic field distribution, the central wavelength of different order mode fields is confirmed. Taking FR3 and FR4 as examples, results in Figure 2b show that the asymmetry caused by the eccentricity is nonlinear to the center wavelength of different orders. With the gradual increase in the degree of eccentricity, the maximum transmittance of different orders will also decrease slightly, and the linewidth will be slightly widened. When the eccentricity is less than 40% (i.e., below 20 nm), the effect of this change on the center wavelength and line width is slight. Since the etching accuracy is in the sub-10 nm range, the effect of this wavelength shift due to eccentricity on the system can be ignored.

We next discuss the effect of the direction of the eccentric ring resonator on the transmission pattern at 60° intervals, and the results show that the eccentric direction does not change the transmission spectrum, which is physically intuitive. All this shows that our compact structure has excellent resistance to eccentricity.

In Figure 3a, we changed the refractive index of the medium in the MUS region and studied the effect of the refractive index on the transmission spectrum. The results show that the maximum value of each Fano formant is redshifted with the increase in the refractive index. Figure 3b–e shows that the linearity of this redshift is very high, making it ideal for use as a sensor. Figure 3g–n shows the magnetic field distribution of different orders at the peaks and valleys of Fano resonance.

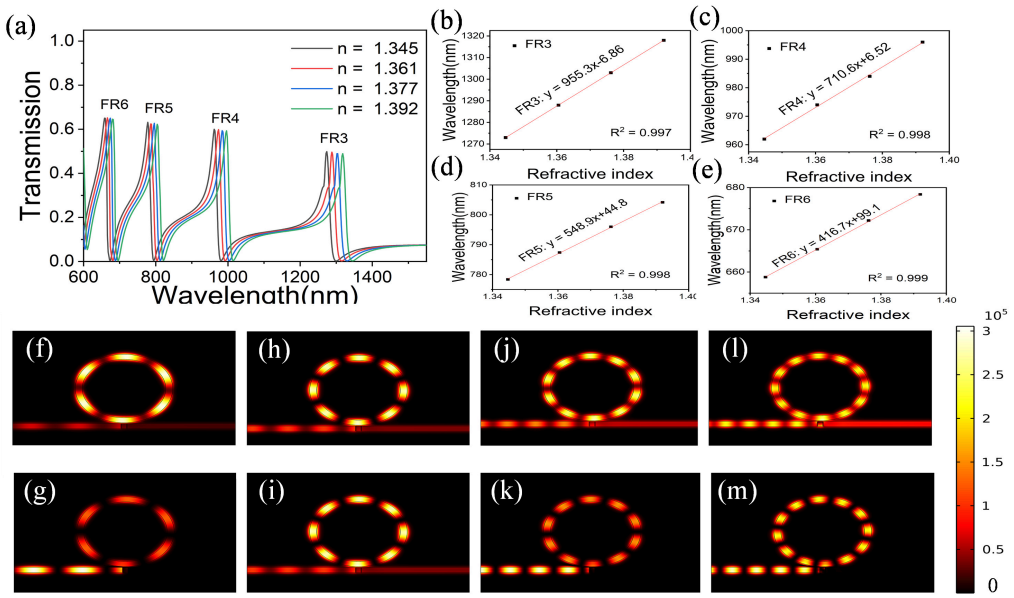

Figure 3. (**a**) Transmittance spectra of the optimized structure for different refractive indices of MUS, n = 1.345 to 1.392. Relationships between the resonance wavelengths of (**b**) FR3, (**c**) FR4, (**d**) FR5, (**e**) FR6, and temperature. $|Hz|^2$ distribution of the peak and valley wavelength in transmittance spectra when T = 60 °C, (**f**) FR3, λ_{peak} = 1274 nm; (**g**) FR3, λ_{valley} = 1300 nm; (**h**) FR4, λ_{peak} = 962 nm; (**i**) FR4, λ_{valley} = 981 nm; (**j**) FR5, λ_{peak} =778 nm; (**k**) FR6, λ_{valley} = 794 nm; (**l**) FR6, λ_{peak} = 659 nm; (**m**) FR6, λ_{valley} = 674 nm.

3.2. Nano-Cylinder-Added Ring Resonator

Maintaining high sensitivity and high FOM in MIM structures is challenging. Adding stubs and grooves to the cavity increases sensitivity but tends to decrease FOM simultaneously. Presently, the sensitivity of sensors based on the MIM ring resonator structure is mainly in the range of 1000–2000 nm/RIU. The FOM of the MIM structure with its sensing accuracy around 3000 nm/RIU is usually around 10 [12,13,20]. Herein, we effectively increased the sensitivity without reducing its FOM by introducing a grating effect into the cavity. We added silver cylinders in the ring resonator, as is shown in Figure 4a, and studied the effect of increasing the silver cylinders on the entire system from two dimensions. First, we studied the changes caused by the silver cylinders at different intervals to the silver

cylinder transmission spectra. The distribution of the magnetic field confirms the order of these modes. We conclude that the grating effect occurs when the distance between the two silver columns is within three times the radius of the silver column.

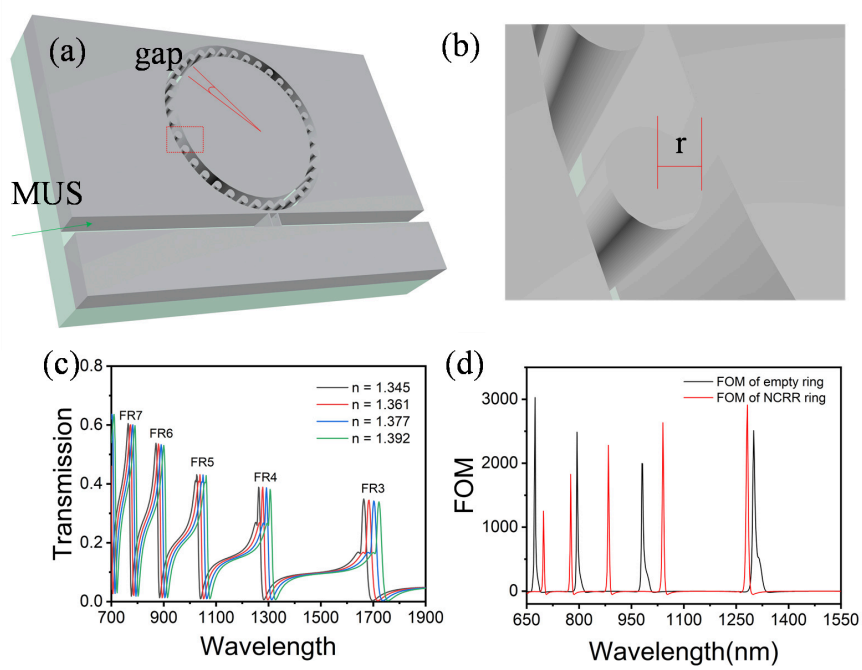

Figure 4. The proposed nanosensor in (**a**) 3D schematic and (**b**) its partial enlargement. (**c**) Transmittance spectra of the NDRR sensor, when radius of the silver cylinders r = 5 nm and intervals of the silver cylinders are 90°. (**d**) FOM of the NDRR sensor and empty ring sensor.

On the other hand, since the width of the ring is 50 nm, we designed three sets of silver cylinders with different radii from 5 nm to 15 nm and studied the effect on the different silver cylinders' radii. The effective refractive index n_{eff} of the pattern increases significantly with the composition of silver increased in the toroidal resonator, so the resonance wavelength position of the same order is significantly redshifted. The effect of sensitivity improvement and the increase in the radius of the silver cylinder present a nonlinear relationship, such that sensitivity improvement after a diameter of 15 nm is not apparent. From this point of view, the sensitivity S is increased up to 42.3%. Additionally, the figure of merit (FOM) = $\triangle T/\mathrm{T}^{*}n$ of the presented schematic is defined. The FOMs of FR3, FR4, FR5, FR6 are 1827, 2280, 2633, and 2911, respectively. Figure 4c shows the transmission pattern when the intervals are 10 degrees and the radius is 15 nm, and Figure 4d shows that the FOMs of these Fano resonances in the structure. The results in Table 3 show that increasing sensitivity slightly increases its FOM, which is rare in other structures [21–24].

Table 3. Summary of the sensitivity for different order modes in different structures. FOM is presented when r = 15 nm and gap interval is 10°.

	FR3 (nm/RIU)	FR4 (nm/RIU)	FR5 (nm/RIU)	FR6 (nm/RIU)	FR7 (nm/RIU)
Empty Ring	955.3	710.6	548.9	416.7	
Gap 30°	980.9	721.3	602.1	466.0	
Gap 45°	972.3	720.1	605.4	477.6	
Gap 90°	961.7	727.7	619.1	474.5	
R = 5 nm	987.2	740.4	608.5	480.9	
R = 10 nm	1061.7	814.9	644.7	557.4	468.1
R = 15 nm	1246.8	951.1	780.9	648.9	553.2
FOM	1251.6	1827	2280	2633	2911

3.3. Potential as a Temperature Sensor

Due to compactness, immunity to electromagnetic interference, wide sensing range, dependability, and high sensitivity, plasmonic temperature sensors are rapidly displacing traditional temperature measurement devices. This ring-shaped resonator is highly sensitive to the refractive index, which makes it perfect for sensing [6,20]. To assess the structure practically, we took temperature as an example. Compared with other optical sensors, the proposed structure has excellent advantages in miniaturization and integration. The refractive index of ethanol can be expressed as

$$n_{\text{Ethanol}}(T) = 1.36048 - 3.94 \times 10^{-4}(T - T_0) \quad (3)$$

where T_0 is the typical room temperature (20 °C) and T is the temperature of the liquid [12]. Ethanol melts at −114.3 °C and boils at 78.4 °C, making it suitable for temperature sensing. Figure 5 plots the transmittance profile for T = 20 °C to T = 40 °C with a step of 5 °C. The results show that temperature has a linear relationship with the resonant wavelength, and our proposed temperature has a sensitivity of 1.48 nm/°C.

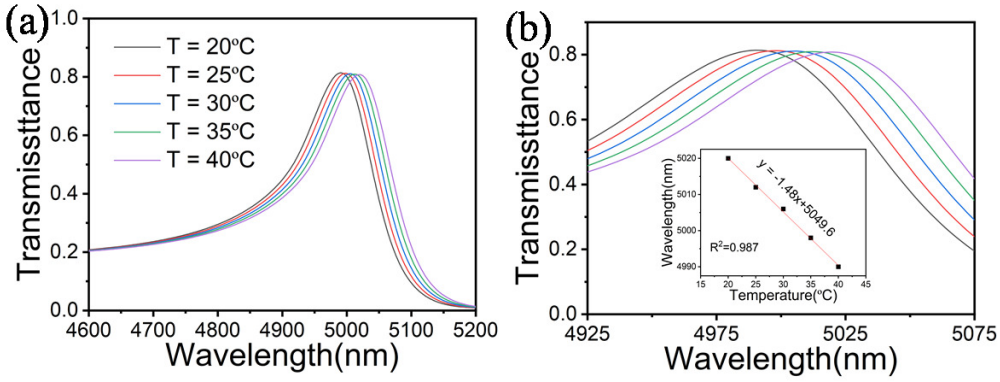

Figure 5. (**a**) Normalized transmittance spectra for NDRR sensor in MIR. (**b**) Enlargement of transmission profile in Figure 5a. The insert figure shows that resonance wavelength increases linearly with temperature.

We compared the accuracy S and FOM of the sensor we designed with the sensing articles of the relevant articles that have been published before, as shown in Table 4. A high sensitivity of 3636.4 nm/RIU as well as a high FOM of 2000 has been achieved in our proposed structure, which shows that the proposed sensor has advantages over others.

Table 4. Comparison of sensitivity with recent literature. Sensitivity data converted to temperature sensitivity use ethnol as the MUS.

Reference	Sensitivity (nm/RIU)	Sensitivity (nm/°C)	Year
[25]	2162	0.848	2020
[26]	1636	0.641	2022
[27]	1303	0.511	2021
[18]	1050	0.412	2022
[28]	1000	0.392	2022
[29]	2000	0.784	2018
This work	3636.4	1.48	2022

4. Conclusions

In this paper, a MIM high-resolution optical temperature sensor decorated with silver nano-cylinders was proposed and numerically analyzed through the FEM method. The maximum transmittance of different order modes increases linearly with decreasing temperature. At 10-degree intervals around the ring cavity, after decorating the radius of 15

nm silver nanodots, we investigated the correlation between temperature and improved the sensitivity S from 955.3 to 1246.8 nm/RIU while maintaining its FOM at about 3000. A maximum sensitivity of 3636.4 nm/RIU can be achieved in MIR. This paper also studied the effect of eccentricity on the transmittance profile due to the deviation in manufacturing and concluded that this machining error has a nonlinear effect on the spectrum. When the deviation in the machining error is less than 40% (i.e., 20 nm), it has little influence on the maximum transmission wavelength. All these characteristics make the proposed structure suitable for temperature sensing, and we achieve a temperature sensitivity of 1.48 nm/°C in MIR. Due to this high sensitivity to temperature, we believe that the structure we designed has essential application prospects in optical switches and all-optical integrated chips.

Author Contributions: P.Z. is responsible for thesis writing and simulations, L.Y. provided theoretical guidance and polished the paper, K.L. and Y.W. helped polish the paper, and Q.S., J.G. and L.J. helped check for paper errors. All authors have read and agreed to the published version of the manuscript.

Funding: National Natural Science Foundation of China (12174037, 12204061, 12204030); Fundamental Research Funds for the Central Universities (2022XD–A09); State Key Laboratory of Information Photonics and Opical Communications (No. IPOC2021ZZ02).

Institutional Review Board Statement: Not applicable.

Informed Consent Statement: Not applicable.

Data Availability Statement: All data are available from the authors upon reasonable request.

Acknowledgments: National Natural Science Foundation of China (12174037, 12204061, 12204030); Fundamental Research Funds for the Central Universities (2022XD–A09); State Key Laboratory of Information Photonics and Optical Communications (No. IPOC2021ZZ02).

Conflicts of Interest: The authors declare no conflict of interest.

Abbreviations

The following abbreviations are used in this manuscript:

MIM	Metal-insulator-metal
NCRR	Nano-cylinder-loaded ring resonator
FEM	Finite element method
RI	Refractive index
MIR	Middle-infrared region
MUS	Material under sensing

References

1. Truong, C.D.; Van, T.N.; Trinh, M.T.; Manh, H.C.; Tan, H.N.; Hoai, B.D. Triple-wavelength filter based on the nanoplasmonic metal-insulator-metal waveguides. *Opt. Quantum Electron.* **2021**, *53*, 223. [CrossRef]
2. Pooretemad, S.; Malekijavan, A.; Aslinezhad, M. Ultrawideband bandstop filter based on Fano resonance and rectangular resonators. *Appl. Opt.* **2021**, *60*, 4266–4272. [CrossRef] [PubMed]
3. Liu, Z.; Gao, Y. Tunable ultra-narrow band band-stop filter based on metal–insulator–metal plasmonic waveguide with square resonator. *Opt. Commun.* **2021**, *501*, 127395. [CrossRef]
4. Ghasemi, M.R.; Bayati, M.S. Proposal for metal–insulator–metal plasmonic power splitter and demultiplexer suitable for implementation in optical switches. *IET Optoelectron.* **2021**, *15*, 200–206. [CrossRef]
5. Rakhshani, M.R. Refractive index sensor based on dual side-coupled rectangular resonators and nanorods array for medical applications. *Opt. Quantum Electron.* **2021**, *53*, 232. [CrossRef]
6. Khonina, S.; Kazanskiy, N.; Butt, M.; Kaźmierczak, A.; Piramidowicz, R. Plasmonic sensor based on metal-insulator-metal waveguide square ring cavity filled with functional material for the detection of CO_2 gas. *Opt. Express* **2021**, *29*, 16584–16594. [CrossRef]
7. Karimi, Y.; Kaatuzian, H.; Tooghi, A.; Danaie, M. All-optical plasmonic switches based on Fano resonance in an X-shaped resonator coupled to parallel stubs for telecommunication applications. *Optik* **2021**, *243*, 167424. [CrossRef]
8. Srivastava, A.; Verma, A.; Prajapati, Y.K. Theoretical study of hazardous carbon-di-oxide gas sensing using MIM structure-based SPR sensing scheme. *IET Optoelectron.* **2021**, *15*, 167–177. [CrossRef]

9. Wang, Y.; Li, S.; Zhang, Y.; Yu, L. Independently formed multiple Fano resonances for ultra-high sensitivity plasmonic nanosensor. *Plasmonics* **2018**, *13*, 107–113. [CrossRef]
10. Shen, S.; She, S.; Wang, Z.; Tan, Q.; Xiong, J.; Zhang, W. MIM waveguide structure consisting of two triangle stubs, side-coupled with an eight-like resonant cavity. *Opt. Commun.* **2021**, *495*, 127087. [CrossRef]
11. Heenkenda, R.; Hirakawa, K.; Sarangan, A. Tunable optical filter using phase change materials for smart IR night vision applications. *Opt. Express* **2021**, *29*, 33795–33803. [CrossRef]
12. Rashid, K.S.; Tathfif, I.; Yaseer, A.A.; Hassan, M.F.; Sagor, R.H. Cog-shaped refractive index sensor embedded with gold nanorods for temperature sensing of multiple analytes. *Opt. Express* **2021**, *29*, 37541–37554. [CrossRef]
13. Butt, M.; Khonina, S.; Kazanskiy, N. A compact design of a modified Bragg grating filter based on a metal-insulator-metal waveguide for filtering and temperature sensing applications. *Optik* **2022**, *251*, 168466. [CrossRef]
14. Zegaar, I.; Hocini, A.; Ben salah, H. In *Journal of Physics: Conference Series, Proceedings of the XXI International Conference and School on Quantum Electronics, Online Event, 21–25 September 2020*; IOP Publishing: Bristol, UK, 2021; Volume 1859, p. 012024.
15. Ji, P.; Shi, Q.; Zheng, L.; Wang, G.; Chen, F. High sensitivity plasmonic refractive index and temperature sensor based on square ring shape resonator with nanorods defects. *Opt. Quantum Electron.* **2022**, *54*, 184. [CrossRef]
16. Faghani, A.A.; Yaghoubi, E.; Yaghoubi, E. Triple-channel glasses-shape nanoplasmonic demultiplexer based on multi nanodisk resonators in MIM waveguide. *Optik* **2021**, *237*, 166697. [CrossRef]
17. Karimi, Y.; Kaatuzian, H. Low-Power Fano Resonance-Based MIM Plasmonic Switch Using Kerr-Type Nonlinear Material. In Proceedings of the 2021 29th Iranian Conference on Electrical Engineering (ICEE), Tehran, Iran, 18–20 May 2021; pp. 32–35.
18. Khani, S.; Hayati, M. Optical sensing in single-mode filters base on surface plasmon H-shaped cavities. *Opt. Commun.* **2022**, *505*, 127534. [CrossRef]
19. Butt, M.A.; Khonina, S.N.; Kazanskiy, N.L. An array of nano-dots loaded MIM square ring resonator with enhanced sensitivity at NIR wavelength range. *Optik* **2020**, *202*, 163655. [CrossRef]
20. Tathfif, I.; Yaseer, A.A.; Rashid, K.S.; Sagor, R.H. Metal-insulator-metal waveguide-based optical pressure sensor embedded with arrays of silver nanorods. *Opt. Express* **2021**, *29*, 32365–32376. [CrossRef]
21. Al Mahmud, R.; Faruque, M.O.; Sagor, R.H. A highly sensitive plasmonic refractive index sensor based on triangular resonator. *Opt. Commun.* **2021**, *483*, 126634. [CrossRef]
22. Hassan, M.F.; Sagor, R.H.; Tathfif, I.; Rashid, K.S.; Radoan, M. An optimized dielectric-metal-dielectric refractive index nanosensor. *IEEE Sensors J.* **2020**, *21*, 1461–1469. [CrossRef]
23. Fan, H.; Fan, H.; Fan, H. Multiple Fano resonance refractive index sensor based on a plasmonic metal-insulator-metal based Taiji resonator. *J. Opt. Soc. Am. B* **2022**, *39*, 32–39. [CrossRef]
24. Chen, J.; Li, J.; Liu, X.; Rohimah, S.; Tian, H.; Qi, D. Fano resonance in a MIM waveguide with double symmetric rectangular stubs and its sensing characteristics. *Opt. Commun.* **2021**, *482*, 126563. [CrossRef]
25. Xu, D.; Yan, S.; Yang, X.; Su, H.; Wu, X.; Hua, E. A Nanoscale Structure Based on a Ring With Matchstick-Shape Cavity for Glucose Concentration and Temperature Detection. *IEEE Sensors J.* **2020**, *21*, 4442–4450. [CrossRef]
26. Rohimah, S.; Tian, H.; Wang, J.; Chen, J.; Li, J.; Liu, X.; Cui, J.; Hao, Y. Tunable multiple Fano resonances based on a plasmonic metal-insulator-metal structure for nano-sensing and plasma blood sensing applications. *Appl. Opt.* **2022**, *61*, 1275–1283. [CrossRef]
27. Li, J.; Chen, J.; Liu, X.; Tian, H.; Wang, J.; Cui, J.; Rohimah, S. Optical sensing based on multimode Fano resonances in metal-insulator-metal waveguide systems with X-shaped resonant cavities. *Appl. Opt.* **2021**, *60*, 5312–5319. [CrossRef]
28. Guo, Z.; Wen, K.; Qin, Y.; Fang, Y.; Li, Z.; Chen, L. A plasmonic refractive-index sensor based multiple Fano resonance multiplexing in slot-cavity resonant system. *Photonic Sens.* **2022**, *12*, 175–184. [CrossRef]
29. Alipour, A.; Farmani, A.; Mir, A. High sensitivity and tunable nanoscale sensor based on plasmon-induced transparency in plasmonic metasurface. *IEEE Sens. J.* **2018**, *18*, 7047–7054. [CrossRef]